Research Square

Preprints are preliminary reports that have not undergone peer review.
They should not be considered conclusive, used to inform clinical practice,
or referenced by the media as validated information.

Calcium, light and the adaptable topography of pectin in the cell wall of the streptophyte alga, Penium margaritaceum

David Domozych

ddomoz@skidmore.edu

Skidmore College https://orcid.org/0000-0001-8800-0061

Josephine G LoRicco

Muhlenberg College

Kaylee Bagdan

Skidmore College Department of Biology

Stuart Malone

Skidmore College Department of Biology

Michael Becker

Skidmore College Department of Biology

Research Article

Keywords: pectin, homogalacturonan, calcium, light, Penium margaritaceum

Posted Date: September 16th, 2026

DOI: https://doi.org/10.21203/rs.3.rs-10842104/v1

License: This work is licensed under a Creative Commons Attribution 4.0 International License.
Read Full License

Abstract

Pectins are major components of the plant cell wall that contribute to multiple foundational functions of the cell. Homogalacturonan (HG) is the most common type of pectin that undergoes significant structural changes when binding to calcium, a mechanism that subsequently alters cell wall dynamics during development and in response to stress. In this study, we employed the unicellular streptophyte alga, *Penium margaritaceum*, to analyze the topography of its unique pectin lattice located on the outside of its cell wall. Using a variety of microscopy-based technologies, we show the sensitivity of lattice architecture to calcium levels. When allowed to recover, the cell uses multiple lattice recovery mechanisms that are parts of uni- and bipolar expansion as well as a repair system. The production of the HG lattice also requires light as it drives the production of photosynthetic carbon for pectin biosynthesis machinery. When placed under an accelerated light dark cycle, the topography of the HG exhibits a banding pattern. This work demonstrates the malleability of HG in response to external chemical and physical signals and the use of this unicellular alga in the study of pectin dynamics of plants.

Introduction

The cell wall (CW) provides multiple integral functions for a plant cell. This complex and dynamic extracellular covering forms a protective rigid barrier, controls growth, expansion and morphogenesis, serves as a prime site of water/mineral uptake and transport, and acts as a conduit for the reception of, and response to external abiotic and biotic stresses (Delmer et al. 2024). The polymers that make up plant CWs constitute the largest source of biomass produced each year on the planet (Bar-on et al. 2018). They also represent the foundations of many industries (e.g. textile, food and biofuels) that yield hundreds of billions of dollars annually (Cosgrove 2024). Over the past decades, research encompassing multiple technologies derived from biochemistry, cell and molecular biology and microscopy, has yielded much insight on the structure, function and development of the CW (Alonzo Baez and Bacete 2023; Besten et al., 2025; Cox and Czymmek, 2025; Daraspe et al. 2025; Zhang et al. 2025; Pu et al. 2025; Zheng et al. 2020). However, many challenges still remain (Delmer et al., 2024; Novaković et al., 2018). For example, elucidating the topography of specific components in the CW complex during the development of a specific cell, especially those in complex tissues and organs, continues to be a major challenge.

Pectins are one of the main CW components that are integral to the architecture and functioning of the CW. These galacturonic acid (GalA)-containing polymers are part of the hydrated CW matrix (Anderson 2016; Caffall and Mohnen 2009), and recently have been shown to play far greater roles in CW dynamics than previously thought (Anderson and Pelloux 2025; Cosgrove 2024). Pectins directly contribute to the modulation of CW mechanical strength, the assembly of the cytokinetic apparatus and the control of CW porosity, ion uptake, CW/cell expansion/development and cell-to-cell adhesion (Obomighie et al. 2025; Anderson and Pelloux 2025; Delmer et al. 2024). Equally important, they also provide a conduit for responding to external abiotic and biotic stressors (Debnath et al. 2026; Molina et al. 2024; Roig-Oliver et

al. 2025; Forand et al. 2022; Liu et al. 2022). Pectic macromolecules are currently classified in several major groups based on the chemistry of their glycan backbones. The most common and well-studied pectin is homogalacturonan or HG that is a homopolymer of α-D-1,4–linked GalA. HG is synthesized in the Golgi apparatus (Hoffmann et al. 2021) and some proportion of the C6s of its GalAs are methylesterified by enzymes of the QUASIMODO (QUA, methyltransferases) family (Wang et al. 2025; Kohorn et al. 2023). The methylesterified HG is transported by secretory vesicles to specific plasma membrane sites and secreted to the CW. Here, pectin methylesterases (PMEs) de-methylesterify the C6s of GalA that now become negatively charged (Anderson and Pelloux 2025). HG chains can then crosslink to each other by binding to Ca^{2+} via a “zipper”-like mechanism (Obomighie et al. 2025; Byun et al. 2019; Kastner et al. 2014). This manifests in the formation of strong gels or nanofibrillar aggregates. The degree and pattern of methylesterification of HG and specific activities of different PMEs determine the biomechanical properties of the HG. The strength of these HG components is also dependent on the amount of Ca^{2+} available for binding to the HG. HG-Ca^{2+} complexes directly contribute to maintaining CW architecture, porosity, water retention and expansion dynamics (Obomighie et al. 2025).

Streptophyte algae are extant green algae that are most closely related and ancestral to land plants (Bierenbroodspot et al., 2024). Many of these algae have been shown to be effective and practical model organisms for a variety of CW studies (Boyer, 2016; Hereburger *et al.*, 2019, Lutz-Meindl, 2016; Proseus and Boyer, 2006, 2012; Domozych *et al.*, 2007, Domozych and LoRicco, 2024). One of the most distinct CWs found in streptophyte algae is that found in the unicellular desmid, *Penium margaritaceum* (Zygnematophyceae). This alga produces a sculpted outer CW layer consisting of Ca^{2+}-complexed pectin (i.e., HG) that sits on an inner CW domain of cellulose and other polymers (Domozych et al., 2014). *Penium*’s unicellular habit allows for direct microscopy-based visualization of CW surface topography in both live and processed (i.e., fixed) cells. CW development in live cells may also be experimentally tested by application of external agents that target specific CW components or subcellular processes (Palacio-Lopez et al., 2024; Domozych et al. 2026). The production of the HG lattice/CW also requires light, i.e., the need of photosynthetic carbon as the building blocks for their construction (Domozych et al., 2014).

In this study, we first examined the effects of various levels of Ca^{2+} on the development and architecture of the HG lattice of *Penium*. Recovery experiments then ensued in order to visualize how the lattice reformed. We then monitored the effects of and altered photocycle on lattice development in order to see if accelerated light/dark phases affected the formation of the lattice.

Materials and Methods

Culture and maintenance

Penium margaritaceum (strain #2640; *Sammlung von Algenkulturen der Universität Göttingen* - Culture Collection of Algae at Göttingen University) was maintained in liquid Woods Hole medium (WH). Cultures were maintained at 20–25°C 16h:8h light:dark cycle with 3.5 klux (74 µmol photons m^{-2} s^{-1}) of cool

white fluorescent light (LoRicco et al., 2024). Subcultures were made weekly and experimental treatments were made with cells from cultures 10–14 days (d) old (log phase).

For the Ca^{2+} treatments, 1 mL aliquots of WH with the following $CaCl_2$ concentrations: 0.25 mM (control), 1.25 mM (5X $CaCl_2$), 7.5 mM (30X $CaCl_2$), 0.025 mM (0.2X $CaCl_2$) or 0.05 mM (0.1X $CaCl_2$) were placed in the wells of a 12-welled non-coated plate (ThermoFisher, USA). 5 ml of 10–14 d old cell suspensions were collected in 15 mL centrifuge tubes and centrifuged at 800 x g for 1 min. The supernatant was discarded and the cell pellet resuspended in 5 mL of WH. The tubes were vortexed and the centrifugation and wash steps were repeated twice more (i.e., Wash protocol). The pellet was resuspended in 250 µL of WH. 25 µL of washed cells were mixed into each well with the varying $CaCl_2$ concentrations and cultured as above.

For recovery experiments, cells were treated as above for 24 h, 48 h, 72 h and 4 d. 500 µL aliquots of treated cell suspension were collected and washed 3x with WH. The cell pellet was resuspended in 1 mL of WH and placed in the well of a 12-welled plate. Recovery conditions were those described above for general culture. After 24 h, 48 h, 72, or 4 d, aliquots of cells were removed and washed (see above) and processed for further studies.

Immunofluorescence labeling

500 µL of cell suspension from individual wells were collected and placed in a 1.5 mL microcentrifuge tube. The tube was centrifuged as above. The supernatant was discarded, the pellet resuspended in WH and the tube vortexed for 10 sec. The cells were then washed twice more. The pellet was resuspended in 500 µL of the monoclonal antibody (mAb), JIM5 (Kerafast, Shirley, Ma., USA; specificity: low esterified HG; diluted 1:20 in WH), vortexed and then the tube placed on a rotary mixer in the dark for 90 min. The tube was centrifuged and wash as above three times. The pellet was then resuspended in 500 µL of goat anti-rat- TRITC secondary antibody (Sigma, diluted 1:75 in WH). Application of a blocking is not necessary. The tube was centrifuged and washed as above three times. Cells were imaged on a Fluoview 1200 confocal laser scanning microscope (Evident; CLSM). A “TRITC” or “FITC” filter were used for CW labeling and chloroplast autofluorescence was imaged using a “TOTO-3” filter. The mAb JIM7 (Kerafast), was utilized for imaging high esterified HG by the method used for JIM5 labeling.

For some recovery experiments, JIM5-labled cells were treated with $CaCl_2$-enhanced WH for 24 h to 4 d, washed and placed in fresh WH for 1, 2 and 4 d (using previously described conditions for control cultures). The cells were then labeled again with JIM5 but using an anti-rat FITC (Sigma) secondary antibody. For labeling of cellulose (and other ß-glucans), control, treated or recovering cells were collected and washed 3X with WH and resuspended in 1 mL WH containing 1µg/mL Calcofluor (Sigma Chemical). Cells were collected after 10 min, washed with WH and imaged using CLSM (see above) using a UV filter set. For some experiments, cells were first labeled with JIM5-TRITC and then labeled with Calcofluor.

Field Emission Scanning Electron Microscopy (FESEM)

Treated and control cells were collected by centrifugation (see above) and the concentrated pellet of cells (15 µL) was rapidly frozen in liquid nitrogen (LN_2) or placed in a -80^oC freezer. The cells were thawed and 25 µL drops were placed in the center of a 48 x 50 mm glass coverslip. A second coverslip was placed on top and the “sandwich” was placed on a table top. The sandwich was pressed together, the glass coverslips were carefully removed and the disrupted cells were placed and washed in a 15 mL centrifuge tubes with deionized H_2O (dH_20). The tubes were centrifuged at 1,000xg for 1 min. The supernatant was discarded and the pellet was dispersed in 5 mL of dH_2O. The tubes were centrifuged and the supernatant discarded. The pellet was resuspended in 500 µL of dH_2O and transferred to a 1.5 mL centrifuge tube. The tube was centrifuged at 1,000 x g for 1 min and the supernatant was gently pipetted off leaving a dense pellet.

Cambridge stubs (Electron Microscopy Sciences, EMS; Ft. Washington, PA., USA) were coated with double sticky carbon tape and 3–5 µL drops of cell pellet are placed on the surface of the double sticky tape. In some cases, the pellets were diluted 10–100 fold to reduce the density of CWs. The stubs were allowed to dry overnight and then sputter with gold-palladium coated for 50 sec. Imaging using secondary electron on a ThermoFisher Quattra S Field Emission Electron Microscope (FESEM) equipped with an UltraDry Premium EDS detector with full quantitative composition analysis. High resolution FESEM imaging involved a secondary electron detector with a 10 kV accelerating voltage, 2.5 spot size, and a 10 mm working distance under high vacuum conditions. The EDS (Energy Dispersive X-ray Spectroscopy) spectrum collection involved a 10 kV accelerating voltage, 5 spot size, and a 10 mm working distance (each spectrum was acquired over 1 min). We used the standardless quantitative analysis mode. The base spectrum and comparing spectrums were normalized by selecting a same energy range within the spectrum background.

EDS analyses were performed on the CWs of 50 cells of each treatment. Ca^{2+} levels (weight %) were obtained for control and treated cells and several inclusive zones at 80,000x for the inner mesh fibers, the projections and altered lattice components. Average values were then obtained for parts of the 50 cells analyzed.

Transmission Electron Microscopy

Control and treated cells were collected and centrifuged. The supernatant was removed and the cell pellet resuspended in 300 µL of WH. Cryofixation by spray freezing and processing for TEM followed the protocol of Domozych et al. (2014). 70–80 nm sections were cut on a Leica EM UC6 ultramicrotome, stained with Uranyless (EMS) and lead citrate and imaged with a Hitachi HT7800 TEM at 120 kV. In order to extract Ca^{2+} from the lattice, some fixed cells were treated for 1 h with 0.1 M EGTA before dehydration and embedding.

Results

P. margaritaceum is a unicellular desmid whose cellular phenotype is an elongate cylinder consisting of two semicells connected at a central isthmus that contains the nucleus (Fig. 1A). The isthmus is the focal point of cell expansion and cell division. *P. margaritaceum*'s CW is distinguished by an outer layer made of the HG lattice. The lattice consists of a series of 80–85 nm wide fibers that branch and fuse to form an organized inner mesh (Fig. 1B). Branches of this mesh occasionally rise up, fuse with other branches to form the lattice projections. When Ca^{2+} is extracted by treating cells with 0.1 M EGTA for 1 h, the inner mesh fiber is shown to consist of dense aggregates of thin fibrils (6.5 nm thick) that label with the mAb, JIM5 (Fig. 1C). This antibody binds to low methyl esterified HG (Claussen et al., 2003; Domozych et al., 2014). Fibrils from the basal areas of the inner mesh fibers extend into the CW's inner domain and aggregate to form the medial layer (Fig. 1D). This layer is encompassed by the network of cellulose microfibrils of the thick inner wall layer. In live cells, JIM5 labels the HG lattice over the entire CW surface except for a narrow band at the isthmus (Fig. 1E). The mAb, JIM7, which recognizes high methylesterified HG, labels this narrow isthmus band (Fig. 1F) and in some cells, it also labels one pole of the cell (Fig. 1G).

FESEM imaging of CW expansion at the isthmus shows that the inner mesh fibers of the lattice emerge from the surface of the inner CW domain and thicken as they expand toward the poles (Fig. 1H). These emergent fibers often align in parallel arrays. The surface of the inner domain of the CW contains ridges that also align in a parallel array (Fig. 1I). Closer examination reveals that the inner mesh fibers emerge from the surface of the ridges (Fig. 1J). EDS analysis of the lattice reveals an increasing amount of Ca^{2+}-binding from the inner mesh to the projections. For example, the projections contain 1.5X the amount of Ca^{2+} than that of the inner mesh fibers (Table 1).

Table 1

EDS analysis of the HG lattice zone upon treatments. Weight% values are provided along with comparative % with control cell lattice. For 30X ca2 + treatment, the surface of the inner domain of the CW where the inner mesh normally is found was analyzed and revealed small amounts of Ca^{2+}.

$CaCl_2$ treatment	***$[CaCl_2]$ mM***	***Ca^{2+} weight % inner mesh***	***Ca^{2+} Weight % projections***	***Ca^{2+}% vs. control inner mesh***	***Ca^{2+}% vs. control projection***
0.1X	0.025	4.3	*No projections*	33.6%	*No projections*
0.2X	0.05	5.8	*No projections*	45.3%	*No projections*
Control (1X)	0.25	12.8	19.2	100%	100%
5X	1.25	13.9	*No projections*	108.6%	*No projections*
10X	2.5	4.0	*No projections*	27.0%	*No projections*
30X	7.5	2.5	*No projections*	19.5%	*No projections*
Light-dark phase				**Ca^{2+}% vs. control inner mesh**	**Ca^{2+}% vs. control projections**
Light		13.3	12.0	103.9%	62.4%
Dark		10.8	10.7	84.3%	55.7%

$CaCl_2$ treatment	*[$CaCl_2$] mM*	*Ca^{2+} weight % inner mesh*	*Ca^{2+} Weight % projections*	*Ca^{2+}% vs. control inner mesh*	*Ca^{2+}% vs. control projection*

Online Resource 1 HG lattice alterations in treatments with 0.25 mM $CaNO_3$ (instead of $CaCl_2$) and co-treatment with 0.25 mM $CaCl_2$ and 0.25 mM $BaCl_2$ or $CaCl_2$ and KCl. a: Altered HG lattice (arrow) in cell treated for 48 h with $CaNO_3$. JIM5 labeling. CLSM image. Bar = 5 µm. b: FESEM image of altered lattice (arrow) in cell treated as in A. Note the irregular components on the CW surface (arrows). Bar = 200 nm. c: Altered HG lattice (arrow) in cell treated for 48 h with equimolar $CaCl_2$ and $BaCl_2$. JIM5 labeling reveals an altered lattice at the expansion zone of the isthmus (I). CLSM image. Bar = 7.5 µm. d: FESEM image of altered lattice in cell treated as in C. Note the irregular components on the CW surface (arrows). Bar = 200 nm. e: Altered HG lattice (arrow) in cell treated for 48 h with both $CaCl_2$ and KCl. JIM5 labeling reveals the altered lattice (arrow) at the isthmus (I). CLSM image. Bar = 7.5 µm. f: FESEM image of altered lattice in cell treated as in E. Note the irregular inner mesh-like components on the CW surface (arrows). Bar = 200 nm

Online Resource 2 Treatments with low $CaCl_2$ (0.025 mM (0.1X) $CaCl_2$ or 0.5 mM (0.2X) $CaCl_2$) and high $CaCl_2$ (2.5 mM (10X) $CaCl_2$). a: When treated for 48 h with 0.05 mM $CaCl_2$ subtle alterations (arrows) to the lattice are observed at the isthmus (I). CLSM image. Bar = 7.5 µm. b: JIM7 labeling of a cell treated with 0.05 mM $CaCl_2$ for 48h. The typical narrow band (arrow) is found at the isthmus (I). CLSM image. Bar = 15 µm. c: FESEM image of the altered lattice in a cell treated for 48 h with 0.05 mM $CaCl_2$. No projections are observed but elongate fibers often in parallel arrays form above the inner meshwork (arrows). Bar = 350 µm. d: JIM5 labeling of a cell treated with 0.025 mM $CaCl_2$ for 48 h. The HG lattice is notably altered (arrow) at the isthmus (I). CLSM image. Bar = 15 µm. e: JIM7 labeling of the more diffuse band (arrow) at the isthmus in a cell treated with 0.025 mM $CaCl_2$. CLSM image. Bar = 7.5 µm. f: FESEM image of the altered CW (AW) highlighting the HG components as irregular tufts (arrow). The cell was treated with 0.025 mM $CaCl_2$ for 48h. Bar = 400 nm. g: Magnified FESEM image of the tufts (arrow) found in a cell treated with 0.025 mM $CaCl_2$. Bar = 180 nm. h: JIM5 labeling of the notably altered HG components of the CW (arrow, AW) of a cell treated for 48 h with 2.5 mM $CaCl_2$ or 10x Ca^{2+}. CLSM image. Bar = 7.5 µm. i: JIM7 labeling of the diffuse band (arrow) at the isthmus of a cell treated with 2.5 mM $CaCl_2$. CLSM image. Bar = 15 µm. j: FESEM image showing the difference of the HG lattice of the pre-existing CW (PW) and the altered HG lattice (arrow) of the altered CW (AW) of a cell treated with 2.5 mM $CaCl_2$. Bar: 1.3 µm. k: Magnified FESEM image of the linear components (arrows) of the altered CW (AW) in a cell treated with 2.5 mM $CaCl_2$. Bar = 500 nm

Online Resource 3 Effects of calcimycin. a: Cell shape changes (arrow) and elongation after 48h treatment in 1 µM calcimycin. Bar = 15 µm. b: After 48 h treatment, JIM5 labels both the altered lattice (arrows) at the isthmus (I) and pre-existing lattice formed before treatment. (CLSM image) Bar = 5 µm. d: FESEM image of the altered lattice (AW, black arrow) in comparison to the lattice of the pre-existing CW (PW, white arrow). Bar = 2.5 µm nm. d: Magnified view of the altered lattice. Note that the “units” if the inner mesh are in linear arrays (double arrows). Bar = 180 nm. e: TEM image of the altered CW zone exhibiting the incomplete lattice (arrows). Bar = 0.5 mm. f: After 48 h recovery from a 48h treatment, JIM5 labels the newly regenerated lattice at the isthmus (I) produced in a bipolar mechanism (white arrows). A new lattice is regenerated at one pole (P, black arrow) by a unipolar mechanism. The altered CW is the repair zone (RZ, black arrow). CSM image. Bar = 10 µm. g: FESEM image of the bipolar synthesis (white arrows) at the isthmus (I) and the repair zone (RZ) in one semi-cell. Bar = 3µm. g: FESEM image of the repair zone after 48 h recovery. Mall projections (arrows) arise from the inner mesh. Bar = 400 nm.

Treatment with elevated Ca^{2+} in the growth medium

We cultured cells in WH containing 5X its normal Ca^{2+} level (i.e., 1.25 mM $CaCl_2$ or 5X the $CaCl_2$ concentration of WH medium). After 48 h treatment, the HG lattice produced at the expanding isthmus is notably altered while the pre-existing wall (PW) lattice (i.e., the lattice of the CW formed prior to treatment) does not visibly change. JIM5 labeling highlights the irregular lattice architecture of the altered wall (AW) at the isthmus (Fig. 2A). The altered zone does not produce the typical lattice but rather is made of irregular components (Fig. 2B). In some cells, the lattice is altered at both the isthmus and at one pole of the cell (Fig. 2C). JIM7 labels a broader and denser band at the isthmus (Fig. 2D) when compared with control cells (see Fig. 1F). Diffuse JIM7 labeling is also often observed at one pole of the cell (Fig. 2E). FESEM imaging reveals that the altered CW zone originates at the isthmus (Fig. 2F) and contains elongate, irregular and thickened fibers (Fig. 2G). No inner mesh is formed (compare with Fig. 1B). After 72 h treatment, even larger irregular components emerge from some of the altered fibers (Fig. 2H). TEM imaging highlights the distinct changes to the CW with irregular electron dense components formed instead of the organized lattice (Fig. 2I). EDS analysis of the altered lattice shows that the level of Ca^{2+} is the same in the inner mesh fibers and altered thickened components (Table 1). The inner mesh fibers and altered components contain slightly more Ca^{2+} (8%) than control fibers. Both though contain considerably less Ca^{2+} than the projections of control cells (i.e., 72.4%).

Cells were also treated with another Ca^{2+} salt, $CaNO_3$ in order to compare topographical changes with that of $CaCl_2$. After 48h treatment, the typical lattice is not present but is replaced by elongate fibers and irregular components (Suppl. Figure 1A, B), similar to that observed with $CaCl_2$ treatment. We also wanted to ascertain if the addition of other cation salts affected lattice development. When treated cells with equal amounts of $BaCl_2$ and $CaCl_2$ for 48h the lattice was replaced by a dense covering of irregular components (Suppl. Figure 1C, D). When treated with equal amounts of the KCl and $CaCl_2$ for 48h, an irregular inner mesh with a few tiny projections was produced (Suppl. Figure 1E, F).

Recovery of HG lattice

We also monitored the recovery of treated cells when they were washed and then allowed to recover in fresh growth medium under normal growth conditions. In all recovering cells a normal HG lattice is produced at the isthmus via the typical bipolar expansion mechanism (Fig. 3A, B). The initiation of lattice formation incorporates fibers emerging from the isthmus center like that of control cells (compare with Figs. 1H, I). In some cells, a second lattice-forming zone appears at one pole of the cell (Fig. 3D, E). In the altered CW zone between the newly formed HG lattices repair of the lattice takes place in a different manner (Fig. 3F). New HG lattice here is not derived from the growing edge of the polar expanding CW/cell. Rather, fibers enter the edges or interfaces of the repair zone with the newly formed HG lattices derived from the isthmus and pole (Figs. 3G, H). Some of these fibers will fuse and form inner mesh like that of control cells. After 4 d recovery, this repair zone contains an expanded inner mesh with an irregular distribution of projections, unlike those of control cells (Fig. 3H).

Treatment with limited Caand high Ca

Cells were also interrogated with other concentrations of Ca^{2+}. First, the alga was incubated in WH medium containing 0.05 mM $CaCl_2$ or 0.2X the concentration of Ca^{2+} in control medium. Subtle JIM5-structural changes to the lattice at the isthmus appear after 48h treatment (Suppl. Figure 2A). JIM7 labels a narrow band at the isthmus (Suppl. Figure 2B) that is similar to that observed in control cells. FESEM imaging of the altered CW zone shows that while the inner mesh of fibers still forms, no projections are made during this treatment (Suppl. Figure 2C). However, parallel-aligned linear arrays of inner mesh fibers form on the CW surface.

When cells are incubated in even lower concentrations of $CaCl_2$ (0.0125 mM of $CaCl_2$ in WH or 0.1X the Ca^{2+} concentration in control medium), more notable changes occur on the altered CW. JIM5 labeling reveals a granular appearance of the HG components at the isthmus in cells treated for 48h (Suppl. Figure 2D) while JIM7 labeling reveals a broader more diffuse band at the isthmus (Suppl. Figure 2E). FESEM imaging of the altered zone shows that the HG lattice is not formed but is replaced by irregular fibrillar tufts (Suppl. Figure 2F). Close-up imaging reveals that these tufts interconnect, often in irregular clusters (Suppl. Figure 2G). EDS analyses of cells treated with 0.1X and 0.2X $CaCl_2$ reveal notable decreases in Ca^{2+} levels (Table 1).

When cells are incubated in WH with 2.5mM $CaCl_2$ (or 10x Ca^{2+}), significant changes to the HG components occur after 48h. JIM5 labeling shows that the typical HG lattice is replaced by a diffuse layer of punctate components (Suppl. Figure 2H) while JIM7 labels a wide band at the isthmus (Suppl. Figure 2I). FESEM imaging reveals that the altered CW is covered by irregular linear components on the surface (Suppl. Figures 2J, K). Ca^{2+} levels drop significantly in the inner mesh of the CW of these treated cells.

The absence of the HG lattice in 30X Ca $^{2+}$ treatments.

Significant alterations to CW architecture occur when cells were incubated in WH containing 7.5 mM $CaCl_2$ (30x the control concentration). After 72 h, a distinct change in cell shape was noted (Fig. 4A). Cells elongate and swell in the cell center unlike control cells and cells studied under previously described Ca^{2+} levels. JIM5 labels just the edges of the central swelling (Fig. 4B). At 4 d or longer incubation, there is little or no labeling in the altered CW zones (Fig. 4C). Once again as with other treatments, some altered cells contain no lattice in the cell center while others were devoid of the lattice at both the isthmus and one pole (Fig. 4D). As with 10x Ca^{2+} treatment, JIM7 labels a broad and diffuse band at the isthmus (Fig. 4E). FESEM imaging of the altered CW zone reveals no lattice-like components on the CW surface. However, linear ridges that run parallel to each other are apparent on the altered CW surface (Fig. 4F, G). TEM imaging also reveals that the ridges on the outer layer of the CW is devoid of any lattice components (Fig. 4I).

Recovery from treatment with 7.5 mM $CaCl_2$ reveals that new lattice is produced at the isthmus in the typical bipolar fashion (Fig. 5A) and displaces pre-existing HG lattice/CW toward the poles (Fig. 5B). In some cells new lattice is fabricated at both the isthmus and at one pole of the cell (Fig. 5C). FESEM imaging shows that after 24 h recovery, the altered CW is covered by irregular components that do not form lattice, indicating the beginning of recovery in this zone (RZ) (Fig. 5D). They appear as fiber-like components that form upon the CW ridges of the altered CW (Fig. 5E). At 48 h recovery, lateral extensions of these fibers emerge, fuse and yield inner mesh-like components (Fig. 5F). After 72 h, branching and fusion of the fibers yield a covering somewhat similar to inner mesh- of the lattice (Fig. 5G). However, projections were never observed in these repair zones.

Effects of calcimycin on lattice development

When cells are treated with the Ca^{2+}-ionophore, calcimycin, notable changes occur. After 48h treatment, the cells elongate and subtle shape changes occur near the isthmus (Suppl. Figure 3A). JIM5 labeling and FESEM analysis after 48 h treatment reveal a distinct change in lattice architecture (Suppl. Figure 3B, C). The altered lattice does not contain projections but has an inner mesh whose “units” form in linear arrays (Suppl. Figure 3D). TEM imaging reveals the small incomplete lattice components of the altered CW (Suppl. Figure 3E). When cells are allowed to recover in fresh medium for 48 h, polar lattice synthesis and repair of the lattice occurs similarly to that found in cells recovering from altered Ca^{2+} levels. In many cells, isthmus-based bipolar lattice synthesis and pole-based unipolar synthesis occur (Suppl. Figure 3F). In between these two new lattices is the repair zone in one semi- cell (Suppl. Figure 3G). Within the repair zone, small projections begin to emerge from the inner lattice (Suppl. Figure 3H).

Effects of altered photocycle on HG lattice production

The production of the CW also requires large amounts of photosynthetically-fixed carbon. In order to monitor lattice/CW production when cells are cultured in light vs. dark, we examined the effects of an accelerated photocycle. Control cells are grown on a 16L-8D cycle while the experimental treatment encompassed a 6L/6D/6L/6D cycle. After 4 D in this accelerated cycle changes to cell shape became apparent (Fig. 6A). The isthmus swells and takes on an irregular contour. JIM5 labeling of the expansion zone at the isthmus reveals a banding pattern in the architecture of HG lattice (Fig. 6B). The number of projections produced during the light phase is greater than that produced in the dark phase. In order to monitor if other CW components were affected by the altered photocycle. When treated cells are labeled both with JIM5 and Calcofluor (i.e., for labeling cellulose, other ß-glucans) the banding is more obvious (Fig. 6C). Calcofluor labeling of control cells alone shows a virtually smooth homogenous surface (Fig. 6D). In treated cells however, banding is obvious in the isthmus zone (Fig. 6E).

FESEM labeling of treated cells also shows that the banding at the isthmus (Fig. 7A). Closer examination reveals the difference in the number and spacing of the projections between CW formed during the light vs. dark phases (Fig. 7B). EDS analyses (Table 1) shows that Ca^{2+} levels of the inner mesh are about the

same as that of control cells but significantly decline in the projections (62.4%). During the dark phases, Ca^{2+} levels were lower in both the inner mesh regions (84.3%) and projections (55.7%).

During recovery (i.e., a return to the normal photocycle) no striations are found in the newly formed lattice at the isthmus or in many cells, at the pole as well (Fig. 7C). However, the banded zone formed during treatment remains. During our examination of over 100 recovering cells, no repair mechanism, like that observed during Ca^{2+} treatments, was apparent.

Discussion

General

HG or HG domains of multi-unit pectins (e.g. HG-Rhamnogalacturonan -I or RG-I) structurally modulate when enzymatic de-methylesterification allows for HG chains to crosslink with the divalent cation, Ca^{2+}, and yield a “zipper” or “eggbox” conformation (Obomighie et al. 2025). This manifests in significant HG architectural transformations and functional modulations that accommodate particular developmental stages of the CW/cell and/or responses to stress. Pectin biosynthesis is also dependent on light and the production of photosynthetically-generated carbon (Falcioni et al., 2020). In order to elucidate changes to the malleable topography of pectin, we employed *P. margaritaceum* with its distinct HG lattice that easily accommodates visualization by various microscopy-based technologies. To do so, we interrogated the alga with different levels of available Ca^{2+} to elucidate HG-Ca^{2+} structural dynamics as well as an accelerated photocycle to examine the role of light in HG lattice formation.

HG lattice formation

The HG lattice of *P. margaritaceum* consists of an inner mesh of interwoven thick fibers that occasionally branch upward and fuse with neighboring branches to form a series of projections. Though not composed of same-sized repeating subunits as that of a true crystalline material, the projections and inner meshwork components exhibit a regular network or lattice on the surface of the CW. When the CW is treated with a chelator (e.g. EGTA) to remove Ca^{2+}, each lattice fiber appears as an aggregate of nanofibrils. These label with the mAb, JIM5, that binds to relatively low esterified HG (Claussen et al., 2003; see also Domozych et al., 2014). This nanofibrillar architecture coincides with observations of pectin from a recent study of *Arabidopsis* pavement cell CWs using three-dimensional direct STochastic Optical Reconstruction Microscopy (3D-dSTORM) and cryo-Scanning Electron Microscopy (cryoSEM; Haas et al., 2020). *P. margaritaceum*’s pectin fibrils measure 6.5 nm in thickness, notably less than those observed in the *Arabidopsis* CW (19–26 nm). This may be due to a lower number of HG chains required for nanofibril formation in the alga’s CW. These nanofibrils are also extensions of unorganized fibrils that reside in the medial CW layer that is embedded in the cellulosic inner layer. The transition of disordered nanofibrils to organized nanofibril aggregates that form the lattice fibers on the CW surface occurs on either side of a narrow band at the isthmus. This band labels with the mAb, JIM7, that binds to high esterified HG (Claussen et al., 2003). This indicates that the nanofibrils are highly esterified in the medial

layer and upon initial emergence onto the CW surface. However, the de-esterification and Ca^{2+}-binding processes must rapidly occur as JIM5, the mAb for low-esterified HG/HG lattice (and Ca^{2+}-linked HG in *P. margaritaceum*), labels the CW of the whole cell except for the band labeled by JIM7. The de-esterifying enzyme, PME, is most likely concentrated at the isthmus band and act as a key regulator for lattice formation. The development of the lattice occurs in a bipolar manner with newly secreted HG displacing pre-existing lattice outward toward both poles of the cell. The identity of the subcellular component(s) that cause HG lattice and CW expansion on two fronts is currently unknown. In other polar growing plant cells, the cytoskeleton plays a key role in directing CW/cell expansion at a growth tip/front (Wang et al., 2016; Kamel and Geitmann, 2023). Previous work with *P. margaritaceum* has revealed bands of cortical cytoskeletal elements, both microtubules and microfilaments, that sit at the isthmus (Ochs et al., 2014). Further work will be required to test whether these subcellular components are responsible for bipolar CW expansion.

In many cells, lattice/CW expansion also occurs at one pole of the cell where new HG lattice/CW displaces pre-existing CW inward. The occurrence of multiple polar expansion mechanisms in a single cell is highly unusual. It may be a result of stress-induced activation of a unipolar expansion leading to expression of a filamentous morphotype (LoRicco et al., 2025; Domozych et al., 2026) from which all desmids are evolutionarily derived. For example, the bipolar lattice/CW expansion mechanism and the positioning of mitosis/cytokinesis at the isthmus represents a type of interstitial growth process found in desmids. However, when stressed, a unipolar pole-based expansion mechanism initiates in order to accommodate CW/cell recovery.

Lattice formation

Our FESEM imaging shows that the HG fibers that emerge onto the outer surface of the CW at the isthmus are initially arranged in a parallel array (Fig. 1H) with approximately 200 nm separation between them. This arrangement of fibers matches the distribution of parallel ridges typically found on the surface of the inner domain of the CW of the isthmus (Fig. 1I). Inner mesh fibers emerge from the surface of the ridges. TEM imaging shows that the ridges are loci where the fibrils of the medial layer connect with the inner mesh fibers on the surface. We posit that the cell deposits high-esterified HG fibrils into the CW that aggregates into the medial layer. At the isthmus, the medial layer organizes in parallel arrays just under the CW surface. During expansion, fibrils from the aggregates emerge onto the CW surface where they organize, de-esterify and crosslink Ca^{2+} to form the mesh fibers (see above). The parallel positioning of the inner mesh fibers is then lost as the cell surface expands during growth, fibers crosslink and project form yielding the typical lattice architecture.

Crosshatching

The alignment of the initial fibers formed at the isthmus and the underlying ridges are parallel to the longitudinal axis of the cell. In a previous study, it was demonstrated that at the isthmus, cellulose microfibrils and an underlying array of sub-PM microtubules are oriented perpendicular to the long axis of the cell (LoRicco et al., 2024). This interwoven arrangement of HG fibrils/cellulose microfibrils may

represent crosshatching of the polymers at the interface of the inner CW domain and the HG lattice at cell's expansion zone. Close interactions between cellulose and pectin have been recognized in studies of plant CWs (Wang et al., 2012). In onion epidermis, a fibrillar pectin network interacts with cellulose fibrils in a mesh-like fashion at the CW surface and also in more distal layers of the CW (Nicolas et al., 2022). Crosshatching of fiber components of the CW significantly enhances the mechanical strength of the CW (Chen at al., 2025). This alignment apportions mechanical stress in multiple directions that makes the CW highly resistant to various physical stresses. In *P. margaritaceum*, crosshatching of the pectin fibers of the inner mesh with the cellulose microfibrils at the surface of the inner CW domain may confer enhanced physical strength at the isthmus. This would help resist turgor pressure at this weakened CW zone (e.g. no or incomplete lattice) and direct cell/CW expansion during morphogenesis leading to the alga's cylindrical shape. Further detailed imaging will be necessary to resolve this.

The malleable HG lattice and availability of Ca^{2+}

When *P. maragritaceum* is incubated in medium with a high concentration of $CaCl_2$ (5X Ca^{2+} of control medium), changes in lattice architecture occur. In the CW/cell expansion zones, the typical lattice does not form but is replaced by irregularly shaped components. The increased availability of Ca^{2+} for HG-binding after de-methylesterification most likely disrupts the ordered assembly of the HG fibrils into the fibers that constitute the lattice. As Ca^{2+} levels are further raised, alterations to the HG lattice become more striking. When cells were incubated in medium with 10X Ca^{2+} (2.5 mM $CaCl_2$), lattice formation is conspicuously curtailed. The typical fibers of the inner mesh and projections do not form but are replaced by small linear components. When cells are incubated in medium with 30X Ca^{2+}, no lattice components formed and the surface of the inner CW domain is naked. It is also important to note that under these high Ca^{2+} levels, CW structural integrity changes morphological changes (e.g. swelling) occur at the expansion zone.

Why do high levels of Ca^{2+} significantly suppress, if not block, the formation of the HG lattice? In plants, increased Ca^{2+} levels have been shown to increase the stiffness of HG gels and may also interfere with the formation of hydrogen bonds leading to large open gaps and fewer interconnections between the HG molecules (Obomighie et al. 2025; Katsner et al. 2014; Byun et al. 2019). This essentially lessens the cohesiveness of Ca^{2+}-HG structures and may likely explain what is observed in *P. margaritaceum*. The excessive amounts of available Ca^{2+} lead to a hyper-binding to HG as it is de-esterified. This then perturbs the formation of HG components and their cohesiveness so that they are physically unable to remain on the CW surface. Likewise, the suppression/inhibition of the HG lattice under high Ca^{2+} levels may be due perturbation of PME activity. PME's processivity typically occurs in a blockwise fashion in that it catalyzes multiple de-methylesterification reactions on a HG chain without releasing the substrate between reactions. High levels of Ca^{2+} have been shown to alter PME processivity (Zhang et al., 2019). Furthermore, excessive Ca^{2+} binding to large numbers of the negatively charged carboxyl groups hinder PME's interaction with the ester bonds, that in turn stops de-methylesterification (Wu et al., 2018; Kumar

et al., 2023; Videcoq et al., 2011; Nari et al., 1991). The specific effects of high Ca^{2+}, i.e., both on structural development of the lattice and the behavior of PME will require further study.

Effects of lower amounts of Ca^{2+}

We also examined the effects of low Ca^{2+}, specifically 0.1X and 0.2X ($CaCl_2$) on the development of the HG lattice. Under 0.1X Ca^{2+} treatment, the typical fibers of the lattice did not form. Rather a series of irregular tufted fibrils cover the altered CW surface. This likely demonstrates that limiting Ca^{2+} level below a certain threshold may suppress crosslinking of HG fibrils and the subsequent formation of the tufts. In cells cultured with 0.2X $CaCl_2$, the lattice fibers form but the typical projections do not. This indicates that the amount of Ca^{2+} is sufficient for the formation of the inner mesh fibers but is inadequate for the production of the projections.

Recovery of HG lattice

When treated cells are washed, placed in WH medium containing the normal amount of $CaCl_2$ (0.25 mM) and then cultured for 48 h or more, the HG lattice is formed by polar synthesis and is also repaired. First, new HG lattice is synthesized by the typical bipolar lattice/CW/cell expansion mechanism located at the isthmus and in many cells, in a unipolar mechanism at one pole of the cell. Both of the synthesis mechanisms displace the altered CW zones formed during a particular Ca^{2+} treatment. This is best observed in cells with both bipolar and unipolar HG lattice synthesis whereby the altered CW is situated between the two synthesis zones. It is at this zone where the altered lattice is not replaced but repaired. At this zone, fibers of new lattice found at the edges of the repair zone penetrate the altered zone where they often make contact with the altered HG components. Branching and fusion of some of these components then yield inner mesh-like components and subsequently, irregular projections. The final product is somewhat different than polar-synthesized lattice but contains a similar architecture to that of the HG lattice. The presence of the repair mechanism illustrates that the cell recognizes an altered or weak zone in its CW and initiates a reinforcement mechanism, i.e., repair, that cannot be performed by typical lattice synthesis from the isthmus or pole. This response to CW stress entails localized perception of cell surface alteration and a redirection of pectin-deposition to the repair zone. Further work will be needed to elucidate the dynamics of the repair process.

During recovery from incubation in 30X $CaCl_2$, new HG fibers are produced on the ridges of surface of the inner domain of the altered CW. This is similar to that observed at the edges of the isthmus during polar expansion. These ridges are most likely parts of the medial layer and represent a source of HG that is used for repair. During repair the HG fibrils emerge onto the CW surface, de-esterify, bind Ca^{2+} and form the new fibers. However, this occurs in a very different manner than the bi- or unipolar lattice synthesis mechanisms. It is intriguing to speculate that these different lattice recovery mechanisms are parts of a complex CW integrity (CWI) maintenance system that recognizes structural stress at different cell surface loci and responds accordingly with different recovery mechanisms.

Effects of the Ca^{2+} ionophore, calcimycin

Calcimycin or A23187 is a polyether ionophore produced by the bacterium *Streptomyces chartreusensis* that is specific for divalent cations like Ca^{2+} (Wu et al., 2018). It affects proton-cation exchange across biological membranes and can flood the cytoplasm with Ca^{2+}. It has been employed as a valuable agent for studying cation dynamics in various subcellular systems (Verma et al., 2011). In this study, 1 µM treatment for 48h results in elongation and subtle shape changes of the cell. While HG lattice formation continues, the product consists of projection-less inner mesh whose units exist in organized linear arrays. It is likely that this calcimycin removes enough Ca^{2+} from the growth medium near the CW that the lattice projections, which contain the highest levels of the cation, cannot form. This limitation might also a drive slower Ca^{2+}-binding to HG that results in the more organized inner mesh patterning.

HG lattice development is affected by photocycle.

Previous studies have shown that CW production is affected by light (Anderson and Hang et al 2025, Wu et al., 2025, Falcioni et al., 2020; Weraduwage et al. 2016, Salazar et al, 2020, 2025) including pectins (Anderson and Pelloux, 2025; Anderson, 2016). This includes not only the amount and quality of light but the photocycle as well. Pectin synthesis, like that for other CW components, requires large amounts of photosynthetically generated carbon (i.e., photosynthate) during CW synthesis and expansion. It is logical to conclude that the rate of pectin production would naturally peak during daylight hours when photosynthesis produces large amounts of carbon (Verbančič et al. 2018). In *P. margaritaceum*, we demonstrate that an accelerated photocycle results in “banding” of the HG lattice. More projections on the lattice are formed during the light phase versus those produced during the dark phase This may be a result of the reduction of photosynthate available during the dark that would then limit the upward branching of inner mesh fibers to yield the projection. Recovery occurs by polar synthesis of the HG lattice at the isthmus and sometimes at one pole. A repair mechanism like that seen with our Ca^{2+} experiments were never observed. The photocycle effects on the lattice were most likely not perceived as stress requiring a special repair process.

Conclusions

This study demonstrates the structural malleability of the HG lattice topography when *P. margaritaceum* is interrogated with different levels of Ca^{2+} or an accelerated photocycle. The ability of CW pectin to respond to these conditions and more importantly, to rapidly recover indicate the critical importance of CW modulations for survival. Modulating CW topography and chemistry were also of paramount importance for ancient zygnematophytes colonizing land and for the evolutionary origin and radiation of early land plants 500 + mya. The distinct topography and easy accessibility of its CW along with incorporating new imaging technologies should make *P. margaritaceum* a practical model organism for investigating pectin dynamics and those of other CW polymers.

Not unlike most studies, our findings result in more questions to be addressed in future: They include: What amount of nanofibrils is needed to form a lattice fiber? What are the geographic and temporal molecular interactions between HG, Ca^{2+} and PME that result first in the formation of the inner mesh and

then, projections? Does fiber expansion stop when Ca^{2+} binding reaches a threshold on a nanofibrillar aggregate? Does the cessation of fiber growth on the CW surface stimulate fiber expansion upward that leads to the formation of projections? What causes fibers to fuse?

Declarations

Competing Interests:

The authors declare that the research was conducted in the absence of any commercial or financial relationships that could be construed as a potential conflict of interest.

Conflict of Interest

The authors declare that the research was conducted in the absence of any commercial or financial relationships that could be construed as a potential conflict of interest.

Funding:

This work was supported by NSF 2129443 (USA).

Author Contributions

DD and JL designed research, participated in data acquisition/analysis and contributed to composition of the manuscript. KB, SM and MB participated in the data acquisition and analyses, and contributed to the writing composition of this manuscript.

Acknowledgments

This work was supported by NSF 2129443 (USA).

Data Availability Statement

The raw data supporting the conclusions of this article will be made available by the authors, without undue reservation.

References

1. Anderson CT, Pelloux J (2025) The Dynamics, Degradation, and Afterlives of Pectins: Influences on Cell Wall Assembly and Structure, Plant Development and Physiology, Agronomy, and Biotechnology. Annu Rev Plant Biol 76:85–113. 10.1146/annurev-arplant-083023-034055
2. Anderson CT (2016) We be jammin': an update on pectin biosynthesis, trafficking and dynamics. J Exp Bot 67:495–502. 10.1093/jxb/erv501
3. Alonso Baez L, Bacete L (2023) Cell wall dynamics: novel tools and research questions. J Exp Bot 2023 74:6448–6467. 10.1093/jxb/erad310
4. Bar-On YM, Phillips R, Milo R (2018) The biomass distribution on Earth. Proc Natl Acad Sci USA 115:6506–6511. 10.1073/pnas.1711842115
5. Besten M, Hendriksz M, Michels L, Charrier B, Smakowska-Luzan E, Weijers D, Borst JW, Sprakel J (2025) CarboTag: a modular approach for live and functional imaging of plant cell walls. Nat Methods 22:1081–1090. 10.1038/s41592-025-02677-4
6. Bierenbroodspot MJ, Pröschold T, Fürst-Jansen JMR, de Vries S, Irisarri I, Darienko T, de Vries J (2024) Phylogeny and evolution of streptophyte algae. Ann Bot 134:385–400. 10.1093/aob/mcae091
7. Byun C, Zheng Y, Pierce A, Wagner WL, Scheller HV, Mohnen D, Ackermann M, Mentzer SJ (2019) The Effect of Calcium on the Cohesive Strength and Flexural Properties of Low-Methoxyl Pectin Biopolymers. Molecules 25(1):75. 10.3390/molecules25010075
8. Caffall KH, Mohnen D (2009) The structure, function, and biosynthesis of plant cell wall pectic polysaccharides. Carbohydr Res 344:1879–1900. 10.1016/j.carres.2009.05.021
9. Chebli Y, Geitmann A (2017) Cellular growth in plants requires regulation of cell wall biochemistry. Curr Opin Cell Biol 44:28–35. 10.1016/j.ceb.2017.01.002
10. Chen S, Burda I, Jani P, Pendrak B, Silberstein MN, Roeder AHK (2025) Fibrous network nature of plant cell walls enables tunable mechanics for development. Nat Commun 16:7565. 10.1038/s41467-025-62844-1
11. Claussen MH, Willats WG, Knox JP (2003) Synthetic methyl hexagalacturonate hapten inhibitors of anti-homogalacturonan monoclonal antibodies LM7, JIM5 and JIM7. Carbohyd Res 338:1797–1800. 10.1016/s0008-6215(03)00272-6
12. Cosgrove DJ (2024) Structure and growth of plant cell walls. Nat Rev Mol Cell Biol 25:340–358. 10.1038/s41580-023-00691-y
13. Cox KL Jr, Czymmek KJ (2025) Plants in the expansion era: recent advances in expansion microscopy in plant systems. J Exp Bot 77:168–177. 10.1093/jxb/eraf327
14. Daraspe J, Bellani E, De Bellis D, Genoud C, Geldner N (2025) Targeted imaging of specialized plant cell walls by improved cryo-CLEM and cryo-electron tomography. Nat Commun 16:11354. 10.1038/s41467-025-66410-7
15. Debnath J, Morton RN, Engelsdorf T, Gigli-Bisceglia N (2026) Plant cell wall remodeling and peptide signaling under abiotic and biotic stress. Plant Commun 7:101741. 10.1016/j.xplc.2026.101741

16. Delmer D, Dixon RA, Keegstra K, Mohnen D (2024) The plant cell wall-dynamic, strong, and adaptable-is a natural shapeshifter. Plant Cell 36:1257–1311. 10.1093/plcell/koad325
17. Domozych DS, LoRicco JG (2023) The extracellular matrix of green algae. Plant Physiol 194(1):15–32. 10.1093/plphys/kiad384
18. Domozych DS, LoRicco JG, Kozel L, Bagdan K, Malone S, Becker M, Bauer L, Buick A (2026) Managing pectin: maintenance of cell wall integrity in the streptophyte alga *Penium margaritaceum*. Ann Bot: mcag107. 10.1093/aob/mcag107
19. Domozych D, Lietz A, Patten M, Singer E, Tinaz B, Raimundo SC (2017) Imaging the Dynamics of Cell Wall Polymer Deposition in the Unicellular Model Plant, Penium margaritaceum. Methods Mol Biol 1563:91–105. 10.1007/978-1-4939-6810-7_7
20. Domozych DS, Sørensen I, Popper ZA, Ochs J, Andreas A, Fangel JU, Pielach A, Sacks C, Brechka H, Ruisi-Besares P, Willats WG, Rose JK (2014) Pectin metabolism and assembly in the cell wall of the charophyte green alga Penium margaritaceum. Plant Physiol 165(1):105–118. 10.1104/pp.114.236257
21. Falcioni R, Moriwaki T, Perez-Llorca M, Munné-Bosch S, Gibin MS, Sato F, Pelozo A, Pattaro MC, Giacomelli ME, Rüggeberg M, Antunes WC (2020) Cell wall structure and composition is affected by light quality in tomato seedlings. J Photochem Photobiol B 203:111745. 10.1016/j.jphotobiol.2019.111745
22. Forand AD, Finfrock YZ, Lavier M, Stobbs J, Qin L, Wang S, Karunakaran C, Wei Y, Ghosh S, Tanino KK (2022) With a Little Help from My Cell Wall: Structural Modifications in Pectin May Play a Role to Overcome Both Dehydration Stress and Fungal Pathogens. Plants Basel 11:385. 10.3390/plants11030385
23. Hoffmann N, King S, Samuels AL, McFarlane HE (2012) Subcellular coordination of plant cell wall synthesis. Dev Cell 56:933–948. 10.1016/j.devcel.2021.03.004
24. Kamel H, Geitmann (2023) Strength in numbers: An isoform variety of homogalacturonan modifying enzymes may contribute to pollen tube fitness. Plant Physiol 194:67–80. 10.1093/plphys/kiad544
25. Kastner H, Kern K, Wilde R, Berthold A, Einhorn-Stoll U, Drusch S (2014) Structure formation in sugar containing pectin gels - influence of tartaric acid content (pH) and cooling rate on the gelation of high-methoxylated pectin. Food Chem 144:44–49. 10.1016/j.foodchem
26. Kohorn BD, Yang N, Weinstock M, Asper G, Ball I, Rajiv D (2023) Golgi ELMO1 binds QUA1, QUA2, GAUT9, and ELMO4 and is required for pectin accumulation in Arabidopsis. PLoS ONE 18:e0293961. 10.1371/journal.pone.0293961
27. Kumar R, Meghwanshi GK, Marcianò D, Ullah SF, Bulone V, Toffolatti SL, Srivastava V (2023) Sequence, structure and functionality of pectin methylesterases and their use in sustainable carbohydrate bioproducts: A review. Int J Biol Macromol 244:125385. 10.1016/j.ijbiomac.2023.125385
28. Liu J, Willick IR, Hiraki H, Forand AD, Lawrence JR, Swerhone GDW, Wei Y, Ghosh S, Lee YK, Olsen JE, Usadel B, Wormit A, Günl M, Karunakaran C, Dynes JJ, Tanino KK (2022) Cold and exogenous

calcium alter Allium fistulosum cell wall pectin to depress intracellular freezing temperatures. J Exp Bot 2022 73:3807–3822. 10.1093/jxb/erac108

29. LoRicco JG, Malone S, Becker A, Xue N, Bagdan K, Eastman A, Sgambettera G, Winegrad A, Gibeau B, Bauer L, Epstein R, Domozych DS (2025) Aberrant growth and expansion in Penium margaritaceum triggered by disruption of microtubules and the cell wall. J Exp Bot 4:961–979. 10.1093/jxb/erae387
30. LoRicco JG, Bagdan K, Sgambettera G, Malone S, Tomasi T, Lu I, Domozych DS (2024) Chemically induced phenotype plasticity in the unicellular zygnematophyte, Penium margaritaceum. Protoplasma 261:1233–1249. 10.1007/s00709-024-01962-x
31. Molina A, Jordá L, Torres MÁ, Martín-Dacal M, Berlanga DJ, Fernández-Calvo P, Gómez-Rubio E, Martín-Santamaría S (2024) Plant cell wall-mediated disease resistance: Current understanding and future perspectives. Mol Plant 17:699–724. 10.1016/j.molp.2024.04.003
32. Nari J, Noat G, Ricard J (1991) Pectin methylesterase, metal ions and plant cell-wall extension. Hydrolysis of pectin by plant cell-wall pectin methylesterase. Biochem J 279:343–350. 10.1042/bj2790343
33. Nicolas WJ, Fäßler F, Dutka P, Schur FKM, Jensen G, Meyerowitz E (2022) Cryo-electron tomography of the onion cell wall shows bimodally oriented cellulose fibers and reticulated homogalacturonan networks. Curr Biol 32:2375–2389e6. 10.1016/j.cub.2022.04.024
34. Obomighie I, Prentice IJ, Lewin-Jones P, Bachtiger F, Ramsay N, Kishi-Itakura C, Goldberg MW, Hawkins TJ, Sprittles JE, Knight H, Sosso GC (2025) Understanding pectin cross-linking in plant cell walls. Commun Biol 8:72. 10.1038/s42003-025-07495-0
35. Ochs J, LaRue T, Tinaz B, Yongue C, Domozych DS (2014) The cortical cytoskeletal network and cell-wall dynamics in the unicellular charophycean green alga Penium margaritaceum. Ann Bot 114(6):1237–1249. 10.1093/aob/mcu013
36. Pu J, Ma J, Zhai H, Wu S, Wang Y, Putnis CV, Wang L, Zhang W (2025) Atomic force microscopy imaging of plant cell walls. Plant Physiol 197:kiae655. 10.1093/plphys/kiae655
37. Roig-Oliver M, Bota J, Flexas J (2025) Pectins as Brakes? Their Potential Implication in Adjusting Mesophyll Conductance Under Water Deficit and Salt Stresses. Plants (Basel) 14:2180. 10.3390/plants14142180
38. Salazar F, Pizarro-Oteíza S, Kasahara I, Labbé M (2022) Effect of ultraviolet light-emitting diode processing on fruit and vegetable-based liquid foods: A review. Front Nutr 9:1020886. 10.3389/fnut.2022.1020886
39. Verbančič J, Lunn JE, Stitt M, Persson S (2018) Carbon Supply and the Regulation of Cell Wall Synthesis. Mol Plant 11:75–94. 10.1016/j.molp.2017.10.004
40. Verma A, Bhatt AN, Farooque A, Khanna S, Singh S, Dwarakanath BS (2011) Calcium ionophore A23187 reveals calcium related cellular stress as I-Bodies: an old actor in a new role. Cell Calcium 50:510–522. 10.1016/j.ceca.2011.08.007

41. Wang Y, Zhang D, Huang L, Zhang Z, Gao J, Liu W, He G, Guo X, Chang S, Hu J (2022) Research Progress of Pectin Methylesterase and its Inhibitors. Curr Protein Pept Sci 23:684–696. 10.2174/1389203723666220919092428
42. Wang H, Zhuang X, Wang X, Law AH, Zhao T, Du S, Loy MM, Jiang L (2016) A Distinct Pathway for Polar Exocytosis in Plant Cell Wall Formation. Plant Physiol 172:1003–1018. 10.1104/pp.16.00754
43. Wang T, Zabotina O, Hong M (2012) Pectin-cellulose interactions in the Arabidopsis primary cell wall from two-dimensional magic-angle-spinning solid-state nuclear magnetic resonance. Biochemistry 51:9846–9856. 10.1021/bi3015532
44. Wang D, Ortega-Salazar IB, Blanco-Ulate B (2025) Homogalacturonan Methylesterification and Cell Wall Regulation: Integrating Biochemistry, Mechanics, and Developmental Signaling for Crop Improvement. Agronomy 15(11):2641. https://doi.org/10.3390/agronomy15112641
45. Weraduwage S, Kim SJ, Renna L, C Anozie F, Sharkey D, Brandizzi T F (2016) Pectin Methylesterification Impacts the Relationship between Photosynthesis and Plant Growth. Plant Physiol 171:833–848. 10.1104/pp.16.00173
46. Wu W, Chen L, Liang R, Huang S, Li X, Huang B, Luo H, Zhang M, Wang X, Zhu H (2025) The role of light in regulating plant growth, development and sugar metabolism: a review. Front Plant Sci 15:1507628. 10.3389/fpls.2024.1507628
47. Wu HC, Bulgakov VP, Jinn TL (2018) Pectin Methylesterases: Cell Wall Remodeling Proteins Are Required for Plant Response to Heat Stress. Front Plant Sci 9:1612. 10.3389/fpls.2018.01612
48. Wu HC, Luo DL, Vignols F, Jinn TL (2012) Heat shock-induced biphasic Ca($^{2+}$) signature and OsCaM1-1 nuclear localization mediate downstream signalling in acquisition of thermotolerance in rice (Oryza sativa L). Plant Cell Environ 35:1543–1557. 10.1111/j.1365-3040.2012.02508.x
49. Zhang H, Xiao L, Qin S, Wan M, Shen F, Zhao J, Li L (2025) Polarized pectin accumulation regulates differential hypocotyl elongation at the dark-to-light transition. Curr Biol 35:699–707e3. 10.1016/j.cub.2024.12.026
50. Zhang L, Gao C, Gao Y, Yang H, Jia M, Wang X, Zhang B, Zhou Y (2025) New insights into plant cell wall functions. J Genet Genomics 52:1308–1324. 10.1016/j.jgg.2025.04.013
51. Zhang L, Wang P, Chen F, Lai S, Yu H, Yang H (2019) Effects of calcium and pectin methylesterase on quality attributes and pectin morphology of jujube fruit under vacuum impregnation during storage. Food Chem 289:40–48. 10.1016/j.foodchem.2019.03.008
52. Zheng Y, Ning G, Cosgrove DJ (2020) High-Resolution Imaging of Cellulose Organization in Cell Walls by Field Emission Scanning Electron Microscopy. Methods Mol Biol 2149:225–237. 10.1007/978-1-0716-0621-6_13

Figures

Fig. 1

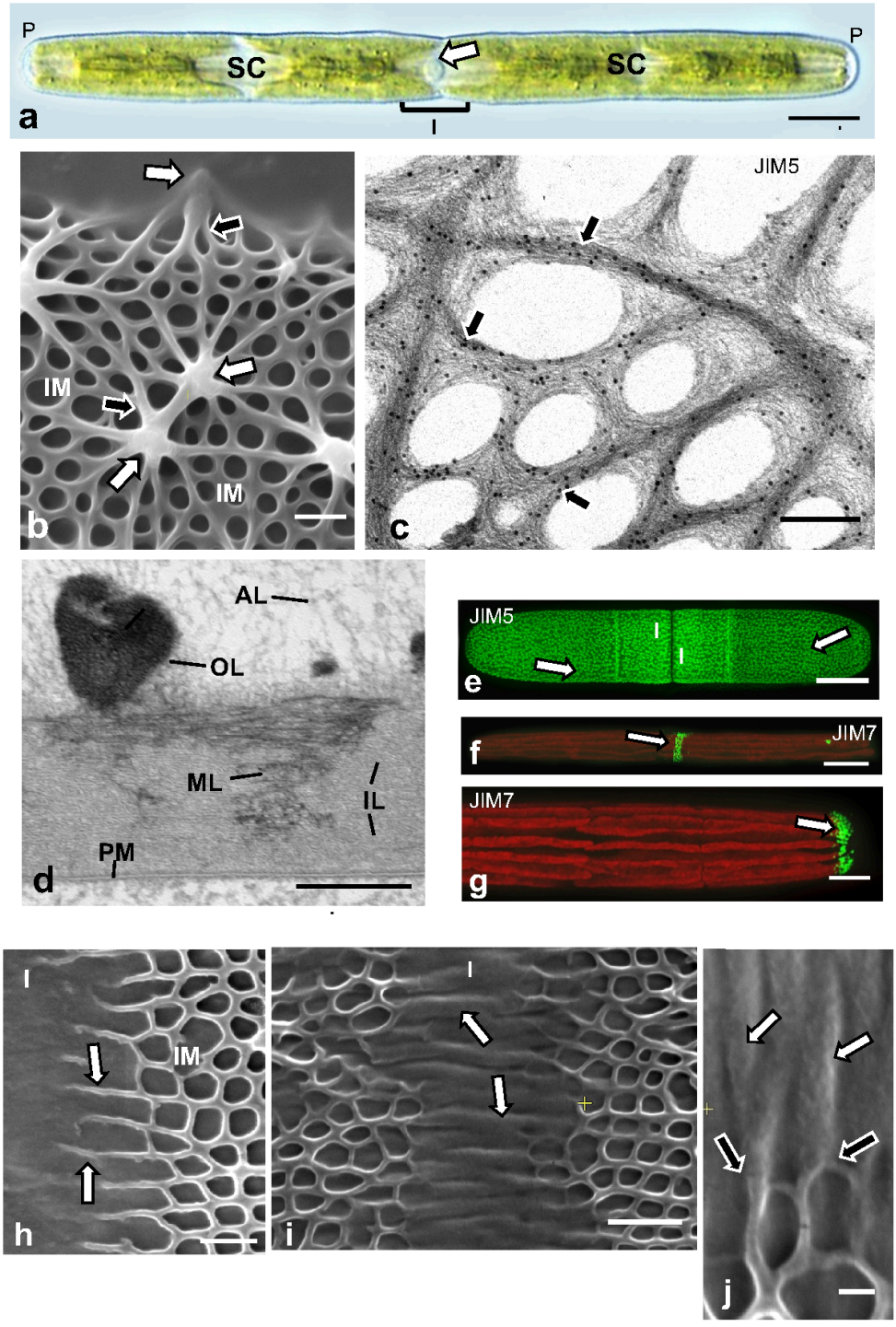


Figure 1

The HG lattice of *P. margaritaceum*. The cylindrical cell consists of two semicells (SC) surrounding the central isthmus (I). The isthmus contains the nucleus (arrow) and is the center of bipolar cell/CW expansion. Bar = 15 µm. b: FESEM imaging shows that the lattice is comprised of an inner meshwork (IM), where branches of the meshwork rise upward (black arrows), fuse with other branches to yield the distinct projections (white arrows). Bar = 360 nm. c: Immunogold/TEM image of the HG lattice labeled

with JIM5. Note the heavy labeling of the lattice fibers (arrows). The section was briefly treated with 0.1 M EGTA to extract Ca^{2+} and reveal the fibrillar components of the lattice fibers. Bar = 180 nm. d: TEM image of the CW. The HG lattice constitutes the outer layer (OL). The outer layer attaches to the medial layer (ML) that is embedded in the inner layer (IL). The plasma membrane (PM) and adhesive layer (AL) are also apparent. Bar = 250 nm. e: JIM5 labeling of the HG lattice (arrows) of a live control cell. (CLSM image. A narrow band at the center of the isthmus (I) is unlabeled. Bar = 7.5 µm. f: JIM7-labeling of the band of high esterified HG (arrow) at the isthmus. Bar = 7 µm. g: JIM7 sometimes labels one pole of the cell (arrow; CLSM image). Bar = 7.5 µm. h: FESEM image of the isthmus (I) where inner meshwork fibers arise (white arrows). Bar = 350 nm. i: FESEM image of the parallel ridges (arrow) found on the surface of the inner domain at the center of the isthmus. Bar = 300 nm. j: FESEM image showing the emergence of the inner mesh fibers (black arrows) from the parallel ridges (white arrows) of the isthmus. Bar = 110 nm.

Fig. 2

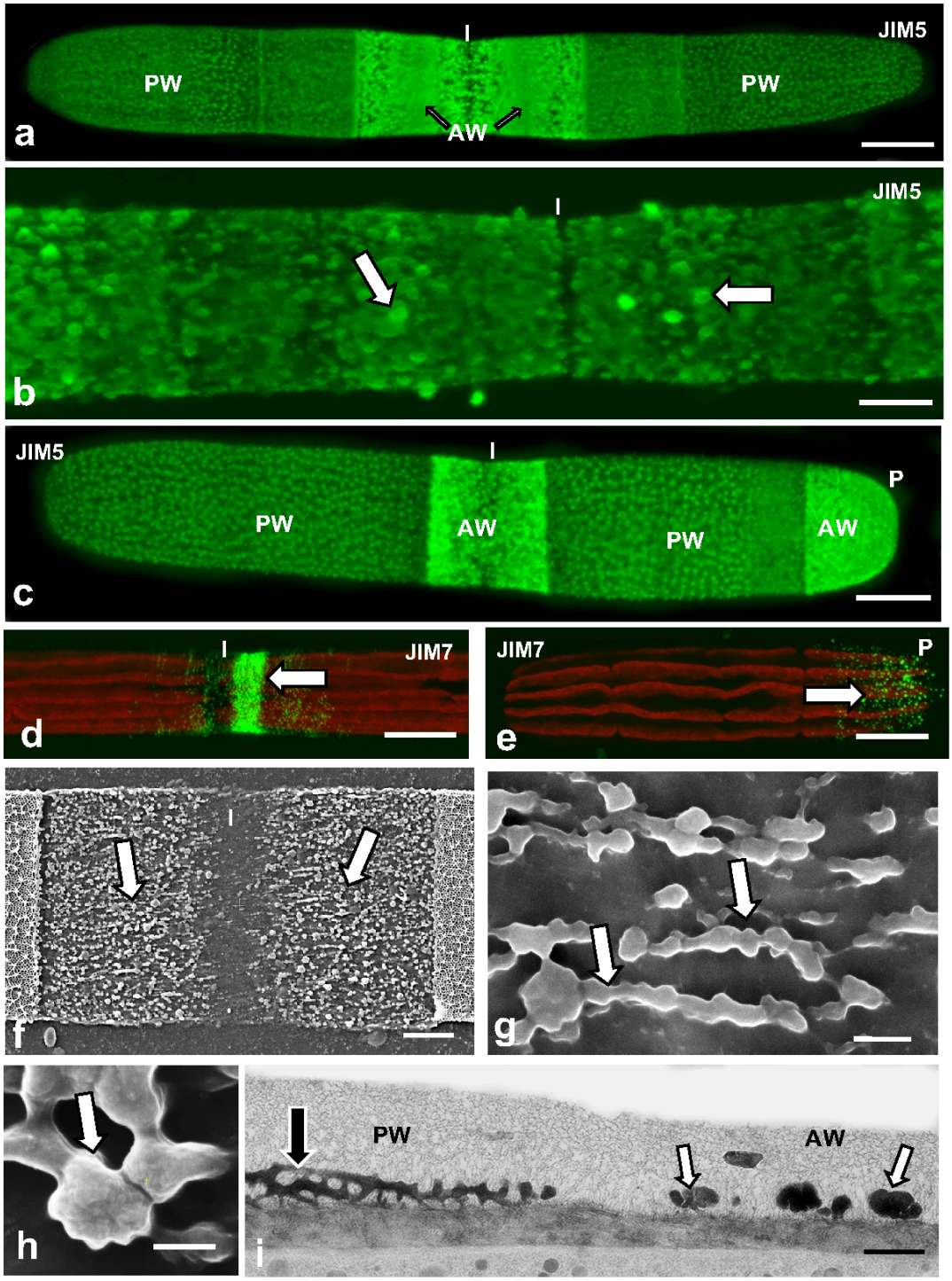


Figure 2

Effects of elevated Ca^{2+}(1.25 mM or 5X $CaCl_2$) on HG lattice structure and formation. a: After 48 treatment a notable change in the structure of the HG lattice at the isthmus is observed when labeled with JIM5. The altered wall (AW) is located on each side of the isthmus (I) and internal to the pre-existing wall (PW). CLSM image. Bar = 7.5 µm. b: Magnified view of the altered CW labeled with JIM5 after 48h treatment. The altered wall at the isthmus (I) consists of HG components of variable size and shape

(arrows). No inner mesh is found. CLSM image. Bar = 5 μm. c: In some cells, the altered wall (AW) formed during treatment can be seen at both the isthmus (I) and also at one pole (P). The pre-existing lattice (PW) is also noted. JIM5-label, CLSM image. Bar = 6 μm. d: JIM7-labeling (arrow) of the band at the isthmus (I) in cells treated for 48h. CLSM image. Bar = 10 μm. e: JIM7- labeling (arrow) of one pole (P) in cells treated for 48h. CLSM image. Bar = 10 μm. f: FESEM image of the irregular HG components now at the isthmus (I). Note the irregular components at the altered zone (white arrows). Bar = 3 μm. g: FESEM image of the altered zone after 48h treatment. Note the irregular, elongate and somewhat thickened linear components (arrows) Bar = 170 nm. h: After 72 h treatment, the altered zone also contains large irregular components (arrow). Bar= 200nm. i: TEM image of the interface between the pre-existing HG lattice/CW (PW, black arrow) and the altered CW (AW). Note the difference between the inner mesh (black arrow) of the pre-existing wall and irregular components (white arrows) found on the altered wall. Bar = 500 nm

Fig. 3

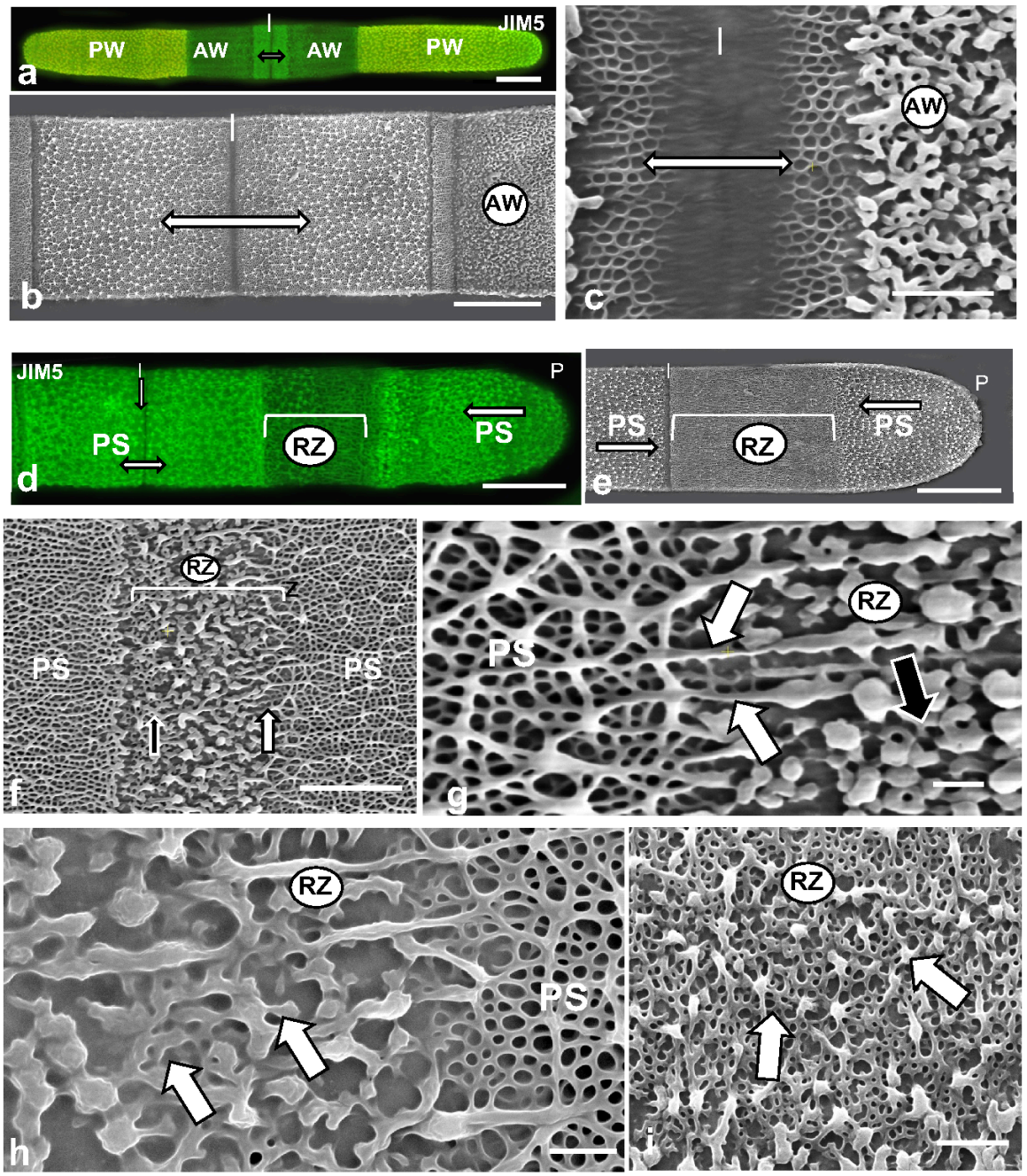


Figure 3

Recovery of HG lattice after treatment with 1.25 mM (5X) $CaCl_2$. a: After 48 h incubation followed by 48 h recovery in fresh medium with 0.125 mM (1X) $CaCl_2$, new HG lattice is formed via bipolar expansion at the isthmus (I, double arrow). The altered CW (AW) and pre-existing CW (PW) are also noted. The cell was labeled with JIM5-TRITC after 48 hours treatment and then with JIM5-FITC after 48 h recovery. CLSM image. Bar = 15 µm. b: FESEM image of the new HG lattice regenerating in the typical bipolar

manner (double arrow) at the isthmus (I) during recovery. The altered CW (AW) is also noted. Bar = 7.5 μm. c: FESEM imaging of the polar synthesis of the new HG lattice at the isthmus in the typical bipolar fashion (double arrow) during recovery (compare with controls, 1H, I). The altered CW (AW) is also noted. Bar = 1 μm. d: In some recovering cells (48h), HG polar synthesis (PS) occurs both at the isthmus (I) and at one pole (P) of the cell. Isthmus-based recovery is bipolar (double arrow) and polar recovery is unipolar (arrow). The repair zone (RZ) is situated between the two polar synthesizing zones. JIM5-labeled. CLSM image. Bar = 7.5 μm. e: FESEM image of a cell recovering as in Fig. 3D. The repair zone (RZ) is positioned between the two polar lattice synthesis zones (PS). Bar = 7.5 mm. f: FESEM image of the repair zone (RZ) located between the two polar synthesized HG lattice zones (PS). Note the interface of the repair zone at the newly synthesized lattice formed at the isthmus (white arrow) and at the pole. Bar = 1μm. g: FESEM image of the repair zone (RZ) at the isthmus-based, polar synthesized lattice zone (PS). Note the elongate fibers emerging from the edge of the synthesized lattice (arrows) and the appearance of small inner mesh-like components (black arrow). Bar = 350 nm. h: FESEM image of the repair zone (RZ) at the edge of the synthesized lattice zone (RL) formed at the pole. Note the inner mesh-like components (arrows) forming in the repair zone. Bar = 180 nm. i: FESEM image of the repair zone (RZ) of cell recovering for 4 d. Note the near normal lattice. The projections though emerge in an irregular pattern (white arrows) off the inner mesh. Bar = 2 μm.

Fig.4

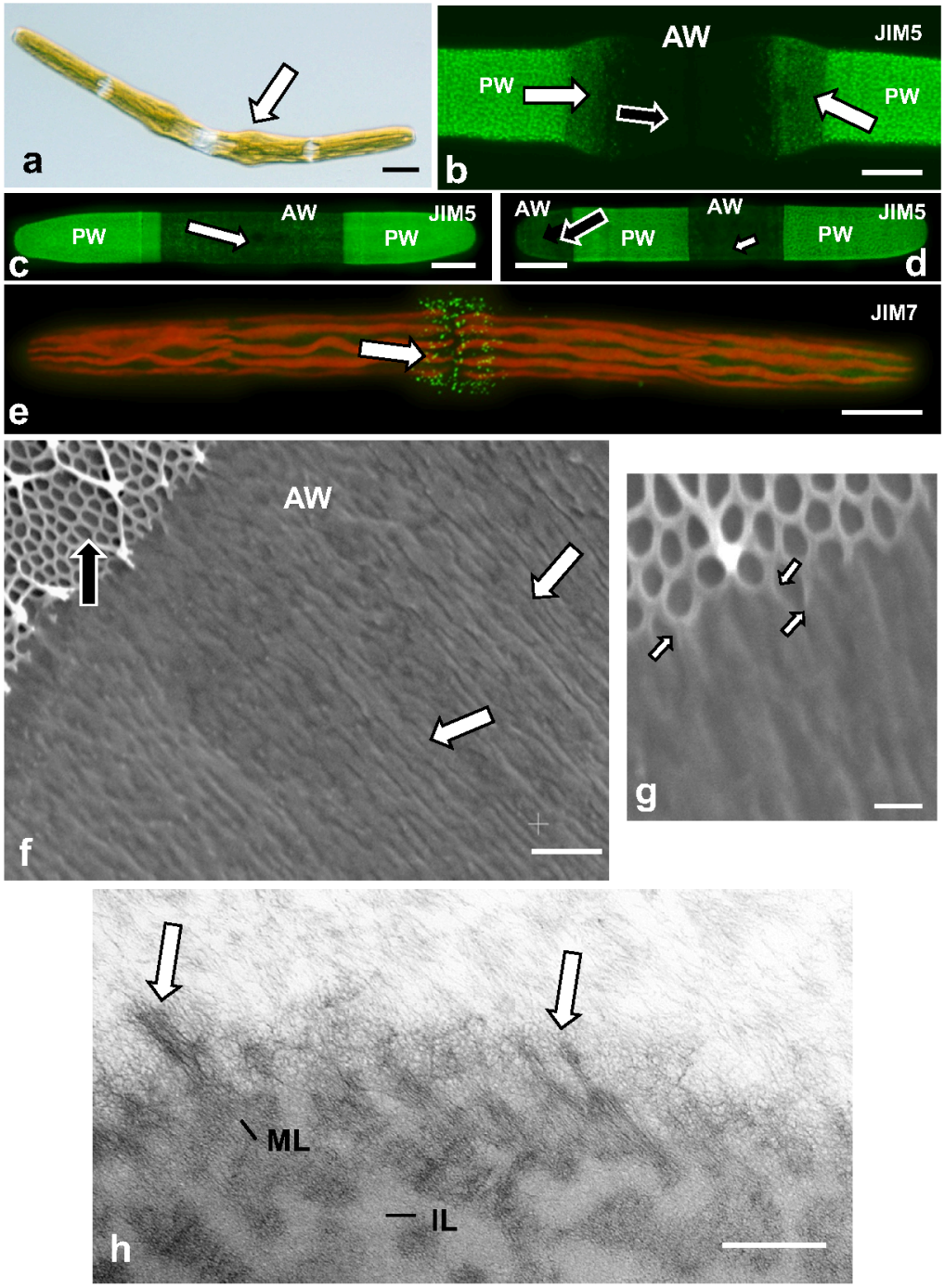


Figure 4

Effects of cells incubated in 7.5 mM $CaCl_2$ (30X Ca^{2+}). a: After 48 h treatment, the cells often elongate and display swollen isthmus zones (arrow). DIC image. Bar = 15 µm. b: After 48 h treatment, JIM5-labeling is weak if not absent in the altered CW zone (AW) at the interface of swollen isthmus (arrows) and the pre-existing CW (PW). CLSM image. Bar = 7.5 µm. c: After 72h, treatment JIM5 labeling of the altered CW (AW, arrow) is absent. The pre-existing CW (PW) is also noted (PW). CLSM image. Bar = 10

μm. d: In some cells after 72h treatment, the altered CW (AW, white arrow) is found at both the isthmus and one pole of the cell (P, black arrow). Bar = 8 μm. e: JIM7 weakly labels a wide zone near the isthmus (arrow). CLSM image. Bar = 10 μm. f: FESEM image of the altered CW (AW). No HG-like components are found. Linear ridges containing (arrows) aligned parallel to each other are found on the CW surface. Bar = 400 nm. g: Magnified FESEM image of the interface between the lattice of the pre-existing CW and the ridges found upon the altered CW of treated cells. Note the connection (arrows) between the inner mesh lattice fibers and the ridges. Bar = 100 nm. H: TEM image of the altered CW zone showing few or no components of the HG lattice (arrows) on the CW surface. The inner (IL) and medial CW (ML) layers are also noted. Bar = 250 nm

Fig 5

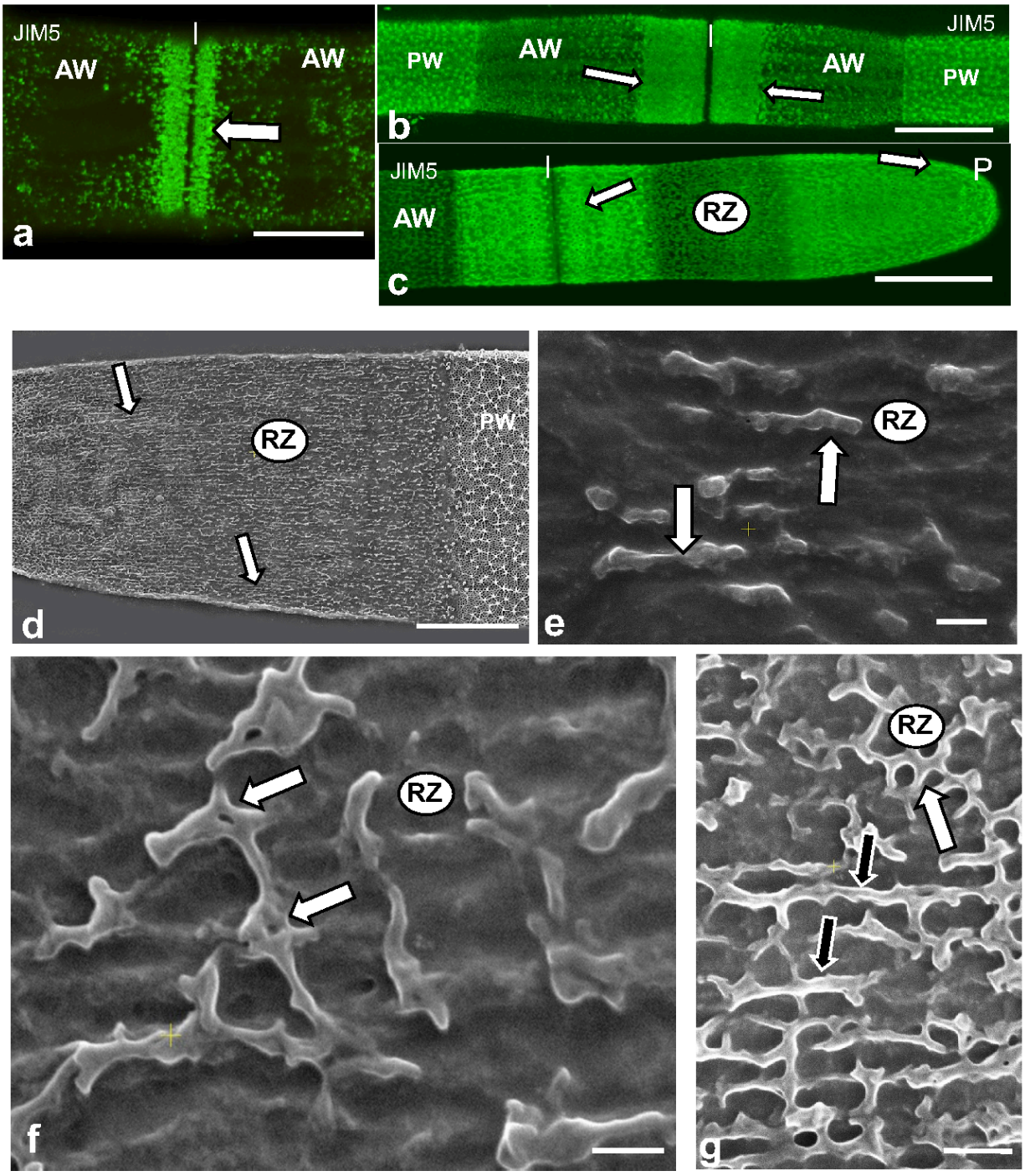


Figure 5

Recovery of HG lattice after incubation in 7.5 mM $CaCl_2$ (30x Ca^{2+}) 7.5 mM $CaCl_2$. a: At 48 h recovery after 72 h incubation, new HG lattice is synthesized (arrow) at the isthmus (I). Altered CW (AW) surrounds this zone. JIM5-labeled. CLSM image. Bar = 7.5 µm. b: The polar synthesis of the HG lattice may be symmetrical during recovery. Bipolar synthesis (arrows) occurs at the isthmus (I) and displaces altered CW (AW) and pre-existing CW (PW) outward. JIM5-labeled. CLSM image. Bar = 15 µm. c: In some

cells, lattice synthesis occurs at the isthmus (I, arrow) and at one pole (P, arrow). The repair zone (RZ) is found between these two synthesis zones. The altered CW (AZ) is also observable. JIM5-labeled. CLSM image. Bar = 15 µm. d: FESEM image of the repair zone (RZ) after 48 h recovery. The typical HG lattice is not formed but the CW surface contains elongate ridges of HG components (arrows). The pre-existing CW is observable. Bar = 5 µm. e: After 24 h recovery, elongate fibers emerge (arrows) from the linear ridges in the repair zone (RZ). FESEM image. Bar = 180 nm. f: After 48 h recovery, the fibers of the repair zone (RZ) start to join together (arrows). FESEM image. Bar = 250 nm. g: After 72 h recovery, the fibers in the repair zone continue to branch and connect (black arrows) and begin to form the inner mesh (white arrow). FESEM image. Bar= 250 nm

Fig 6

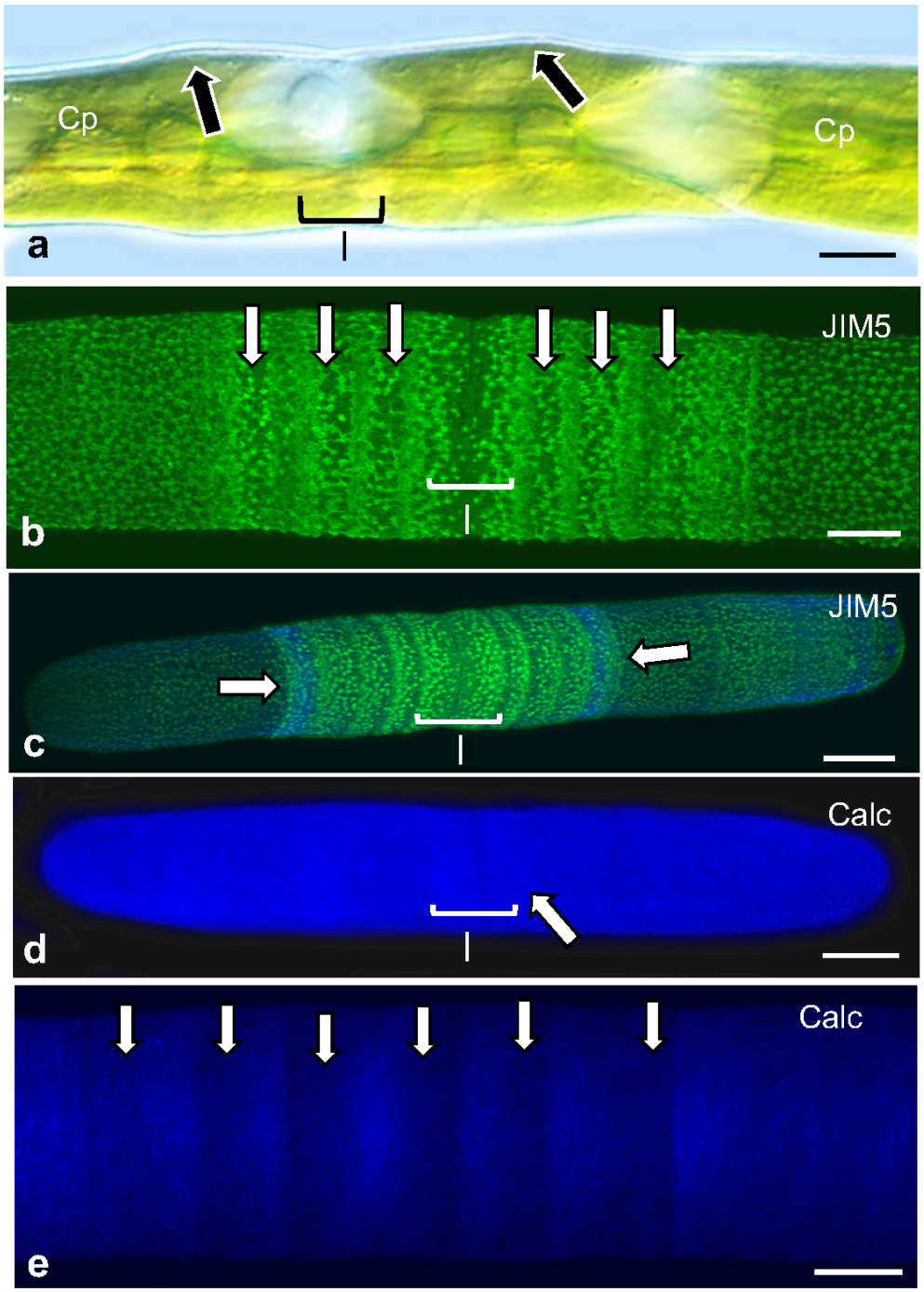


Figure 6

Effects of accelerated photocycle on HG lattice production. a: After 4 d in a 6/6/6/6h L/D/L/D photocycle, cell shape is modified (arrows) at the isthmus (I). Bar= 7.5 µm. b: JIM5 labeling of cell grown for 4 d under the altered photocycle. Note the HG lattice banding (arrows) at the isthmus (I). The lattice produced during the dark are highlighted (arrows). CLSM image. Bar = 5 µm. c: JIM5-Calcofluor co-labeled cell showing the banding of the HG lattice after incubation for 4 d under an altered photocycle.

The isthmus (I) is also noted. CLSM image. Bar= 7.5 µm. d: Calcofluor labeling of a control cell. Note the absence of banding. CLSM image. Bar = 7.5µm. e Calcofluor labeling of an altered cell (4 d incubation). Note banding of the labeling. CLSM image. Bar = 5 µm

Fig. 7

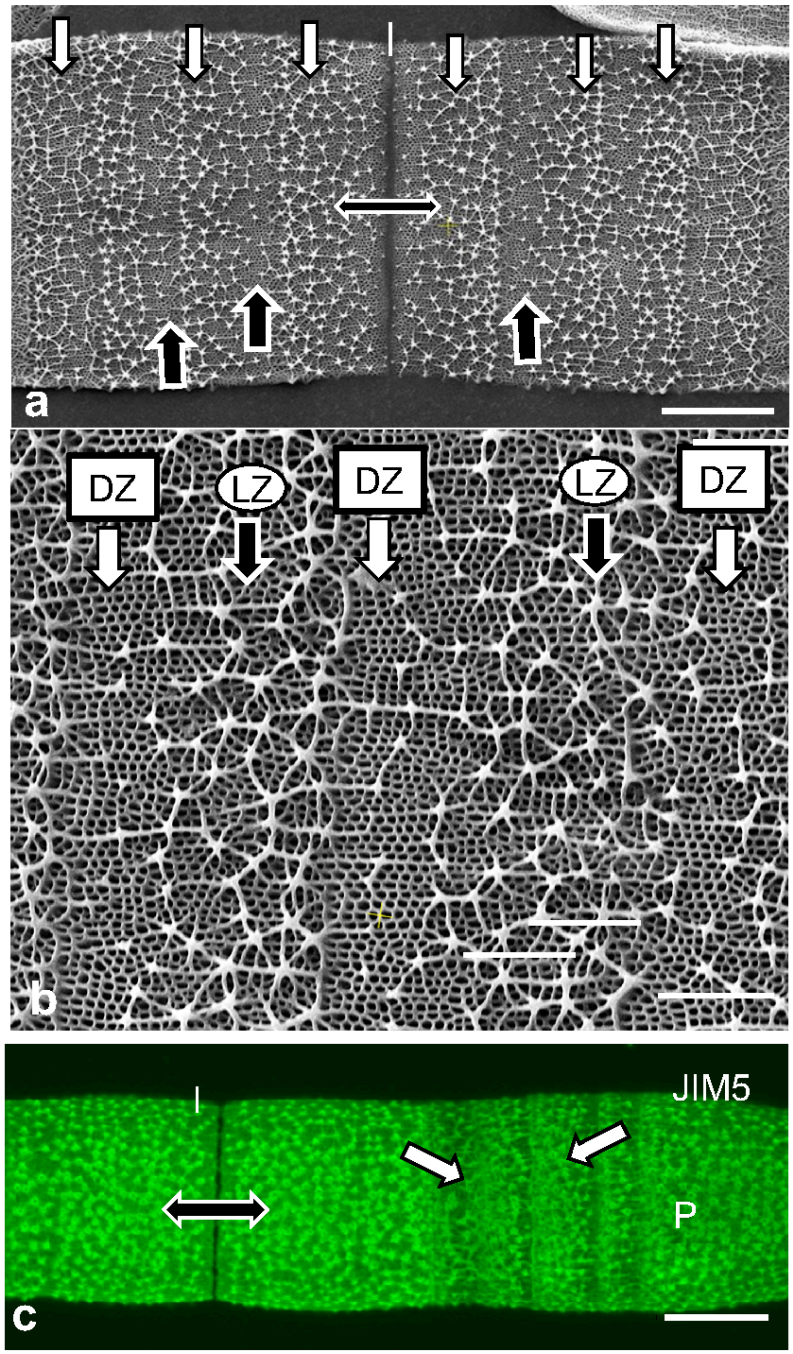


Figure 7

Recovery from altered photocycle. a: 48 h after cells were returned to the normal photocycle, new HG lattice is produced at the isthmus (I). The lattice formed during the light phase (white arrows) and in between the dark phase (black arrows) define the altered CW. FESEM image. Bar = 5 µm. b: Magnified FESEM image of the lattice formed in the dark phase (DZ white arrows) and the light phase (LZ, black arrows). Note the higher number of projections in the lattice produced during the light phase. 2.5 µm. c: Recovery of cell returned to normal photocycle for 48h. JIM5 labeling the synthesis of the lattice by bipolar expansion (double arrow) at the isthmus (I) and unipolar expansion at the polar zone (P). The layered altered lattice remains white arrows). CLSM image. Bar = 7.5 µm

Supplementary Files

This is a list of supplementary files associated with this preprint. Click to download.

- DomozychPeniumonlineresourceplates.pdf